Analysis of Breakthrough Dynamics in Rectangular Channels of Arbitrary Aspect Ratio

Hyungwoong Ahn and Stefano Brandani
Dept. of Chemical Engineering, University College London, Torrington Place, London WC1E7JE, U.K.

DOI 10.1002/aic.10432
Published online May 2, 2005 in Wiley InterScience (www.interscience.wiley.com).

Adsorption in rectangular and square channels is attracting great interest from various fields of research. In particular, in large scale applications the main interest is in the prediction of the performance of monoliths composed of several individual channels, while, in the field of microengineering, particular interest is in the separation performance of individual channels for the development of small-scale analytical devices, that is, the lab on a chip. The design of all these units is based on the accurate representation of the breakthrough dynamics and the performance of the unit can be represented conveniently by the height equivalent to a theoretical plate (HETP). General simplified equations for the calculation of the HETP are derived for rectangular channels of arbitrary aspect ratio. The dispersion in the solid phase is corrected to take into account the effect of the adsorptive capacity in the four corners of the solid phase. A corrected thickness of the walls of the channels is predicted and shown to yield the exact HETP by comparing the analytical solution to the full 3-D numerical solution. Numerical simulations are presented for representative gas and liquid systems. © 2005 American Institute of Chemical Engineers *AIChE J,* 51: 1980–1990, 2005
Keywords: adsorption, rectangular channels, micro-channels, HETP.

Introduction

Structured adsorbents can increase the performance of separation units when compared to traditional packed columns.[1] Monoliths are particularly suitable for rapid cycle pressure swing adsorption (PSA), VOC removal, desiccant cooling and other processes where pressure drop has a significant economic impact.[2] In order to design these units the performance of an individual representative channel is considered, and the theory of Golay[3] is applied. While this can be a reliable tool for qualitative assessments,[1] there is the need for accurate formulations to aid design and development of new processes. This is particularly true in the area of micro-fabricated channels where flow in an open column with rectangular cross section is the basis for the design of microcolumns used as miniature GC and high-speed GC in a variety of practical separation processes.[4]

The separation efficiency in a microfabricated column depends mainly on the size of the rectangular channel and its aspect ratio. Therefore, the effect of channel geometry on the separation performance has been studied widely in liquid chromatography. The starting point for any analysis of these systems is the definition of the Taylor-Aris dispersivity,[5,6] which is a summation of all the effects contributing to the dispersion of solute in the column. Dutta and Leighton[7] identified the effect of various cross-sectional geometries on each term in the Taylor-Aris dispersivity. Zhang and Regnier[8] evaluated the impact of column geometry on the separation efficiency in the electro-osmotic chromatography system through simulations using a three-dimensional (3-D) random walk model. Desmet and Baron[9] showed that the sidewall made a significant contribution to the axial dispersion in liquid chromatography even in rectangular channels with aspect ratios greater than 10.

Since microfabricated columns are made by etching a groove on a silicon wafer, most of these columns have a rectangular cross-section with an aspect ratio greater than 10.[8,10,11,12] Monoliths typically consist of channels with aspect ratios

Correspondence concerning this article should be addressed to S. Brandani at s.brandani@ucl.ac.uk.

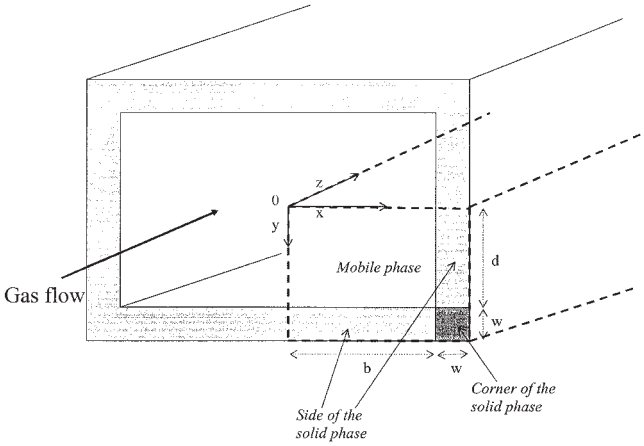

Figure 1. Rectangular channel.

closer to unity. Therefore, the aim of this investigation is the formulation of accurate equations for the calculation of the HETP of rectangular channels of arbitrary aspect ratio.

Golay's pioneering work laid out the mathematical theory for the description of the dispersion of a solute in a channel with laminar flow in the fluid phase and adsorbing walls.[3] Aris[13] treated the same problem for flow in an annular geometry and recovered the limiting case of parallel plates in the limit as the curvature went to zero. Later, Golay[14] improved his model by deriving the approximate expressions from the velocity profile describing the flow field in rectangular channels, introducing an elliptical approximation to estimate the average linear velocity.

More recently Spangler[12] analyzed the same problem using an approximate velocity profile and derived a solution for the HETP of a rectangular gas chromatographic column. Spangler[15] derived a simplified solution for high aspect ratios, recognizing that the dispersion term has an algebraic structure similar to that originally proposed by Golay.[3]

Dutta and Leighton[7] have solved numerically the problem of determining the Taylor-Aris dispersion term using the exact velocity profile. Starting from the problem formulation of Dutta and Leighton,[7] we will derive closed form analytical solutions and simple correlations for the Taylor-Aris dispersion term for rectangular channels of arbitrary aspect ratios and a corrected wall thickness will be introduced to predict accurately the dispersion effect due to mass transfer kinetics in the solid.

Derivation of the HETP Equations

Analytical Analysis

For the rectangular channel shown in Figure 1, the HETP expression for the rectangular column can be expressed as

$$H = \frac{2D_M}{v_{\text{ave}}} + \frac{2k}{3(1+k)^2}\frac{w^2}{D_S}v_{\text{ave}} + \bar{C}_M\frac{4d^2}{D_M}v_{\text{ave}} \tag{1}$$

where v_{ave} is the average velocity, and the partition coefficient k is obtained from $k = K(1-\varepsilon)/\varepsilon$, with K the Henry law constant.

The spread of the solute in the mobile phase along the channel is caused by three mechanisms as described by Eq. 1. The first term on the righthand side is the dispersion of the solute due to axial diffusion. The second term in the expression arises from the diffusional resistance in the solid phase, and the third term is due to the differences in the axial solute velocity resulting from the shear flow in the mobile phase and the retentive force at the wall.

The last term in Eq. 1 is dependent on the flow field and gives rise to a complex formulation for a rectangular channel. Dutta and Leighton[7] have shown that the solution can be represented by

$$\bar{C}_M(k) = \frac{1}{6}\left(\frac{k}{1+k}\right)^2 g_1(\alpha) + \frac{1}{105}g_2(\alpha) + \frac{1}{15}\left(\frac{k}{1+k}\right)g_3(\alpha) \tag{2}$$

where the functions are normalized so they reduce to the limiting case of parallel plates and g_1 accounts for the contribution to dispersion if the velocity profile is uniform, g_2 accounts for the dispersion if there is no adsorption on the walls, and g_3 represents a mixed term. All three functions are only dependent on the aspect ratio α. The function g_1 is[7]

$$g_1 = \frac{2\alpha^2}{(\alpha+1)^2} \tag{3}$$

The functions g_2 and g_3 where calculated numerically by Dutta and Leighton[7] and we have derived the exact analytical solutions which are given in Appendix A. Since the exact solutions of g_2 and g_3 are in terms of infinite series, it is useful to obtain also accurate approximations to these functions that allow a simple way to calculate the HETP

$$g_2 \approx \frac{(7.951-1.759)(\alpha-1)^2}{(\alpha-0.1)^2} + 1.759 \tag{4}$$

$$g_3 \approx \frac{(4.151-0.938)(\alpha-1)^2}{(\alpha+0.2)^2} + 0.938 \tag{5}$$

Figure 2 shows the comparison between the full analytical solutions and Eqs. 4-5.

It is useful also to express

$$\bar{C}_M = \frac{A + Bk + Ck^2}{96(1+k)^2} \tag{6}$$

and determine the values of A, B, C for different aspect ratios. Comparing Eqs. 2-6, it is possible to derive the following identities

$$A(\alpha) = \frac{32}{35}g_2(\alpha) \tag{7}$$

$$B(\alpha) = \frac{64}{35}g_2(\alpha) + \frac{32}{5}g_3(\alpha) \tag{8}$$

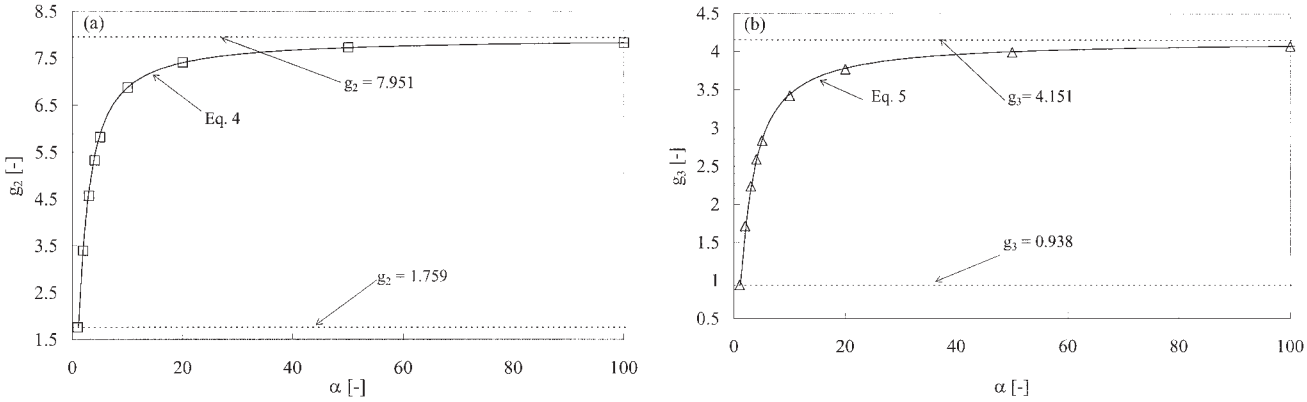

Figure 2. Variation of parameter (a) g_2, and g_3 (b) with the aspect ratio.

$$C(\alpha) = 16g_1(\alpha) + \frac{32}{35}\,g_2(\alpha) + \frac{32}{5}\,g_3(\alpha) \tag{9}$$

Table 1 shows the comparison of our results with other HETP equations for rectangular channels available in the literature. Note that the value of A = 0.9, which is often used, corresponds to the limit of two parallel plates (A = 0.914).

It is worth noting that Figure 2 shows that the side walls have a significant effect even for $\alpha > 10$, a conclusion reached also by Desmet and Baron[9], and that the last term of the HETP equation becomes effectively independent of the aspect ratio only for $\alpha > 50$.

The second term in Eq. 1 represents the dispersion due to Fickian diffusion in the solid phase. This is in principle a three-dimensional (3-D) process, and the formulation presented in Eq. 1 clearly neglects any contribution along the main channel axis, as well as any effect of the aspect ratio.

The axial term may be relevant in the case of a monolith.[17] It is possible to derive a simple order of magnitude estimate of the contribution to the HETP of the axial dispersion through the solid. For this purpose, one can assume a system where the solid phase is always at equilibrium with the gas. Assuming an isotropic material, the 1-D mass balance for a channel can be written as

$$(1 + k)\,\frac{\partial \bar{c}}{\partial t} - (D_M + kD_S)\,\frac{\partial^2 \bar{c}}{\partial z^2} + v_{\text{ave}}\,\frac{\partial \bar{c}}{\partial z} = 0 \tag{10}$$

By inspection of Eq 1, the HETP becomes

$$H = \frac{2(D_M + kD_S)}{v_{\text{ave}}} + \frac{2k}{3(1+k)^2}\,\frac{w^2}{D_S}\,v_{\text{ave}} + \bar{C}_M\,\frac{4d^2}{D_M}\,v_{\text{ave}} \tag{11}$$

Therefore, axial dispersion in the solid phase may become relevant for strongly adsorbed fast diffusing systems at relatively low flow rates.

The diffusion process in the solid phase, at a given axial position, cannot be assumed to be 1-D, especially for small aspect ratios. Because of the symmetries in the channels, the overall diffusional time constant will be close to w^2/D_S, but, because of the four corners, the characteristic time will be longer. The exact value requires a full solution of the problem, and this will be presented in the numerical section. As an approximation, the wall thickness should be corrected in order to yield an equivalent 1-D constant, as shown in Figure 3. In doing this, one must be careful in maintaining the total solid volume constant in order to have the correct retention time for the column. On the basis of these considerations, the simplest approach is to redistribute the solid in the four corners to the four sides of the channels, defining a corrected wall thickness as

$$w_C = \frac{(b + d)w + w^2}{b + d} = \frac{\alpha + 1 + w/d}{\alpha + 1}\,w \tag{12}$$

In typical channels the ratio w/d will be at most 1, so, for channels with high aspect ratios, the corrected thickness becomes the actual wall thickness, as is often assumed,[7,12] while for square channels the maximum deviation is achieved, and the corrected thickness is

$$w_C = \frac{2 + w/d}{2}\,w \tag{13}$$

The HETP equation is rewritten as

Table 1. Comparison of Coefficients for $96(1 + k)^2\bar{C}_M(k) = A + Bk + Ck^2$

	This work		Spangler[15]	Giddings et al.[16]	Golay[3]	
	$\alpha = 1$	$\alpha = \infty$	$\alpha = \infty$	$\alpha = \infty$	Open tubular*	$\alpha = 1$
A	1.608	7.269	0.9	0.9	1	0.9
B	9.220	41.11	2.0	8.2	6	8.2
C	15.61	65.84	35	23	11	23

The hydraulic radius should replace d in the last term of the HETP equation.

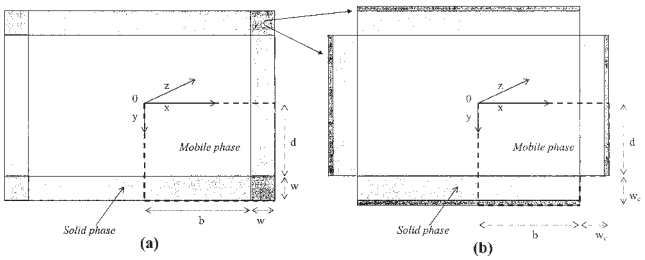

Figure 3. Redistribution of solid from the four corners to the sides: (a) actual system, and (b) system with corrected wall thickness.

$$H = \frac{2(D_M + kD_S)}{v_{\text{ave}}} + \frac{2k}{3(1+k)^2} \cdot \frac{w_C^2}{D_S} \cdot v_{\text{ave}} + \bar{C}_M \frac{4d^2}{D_M} v_{\text{ave}} \quad (14)$$

The validity of Eq. 14 will be tested against a full 3-D numerical solution.

Numerical Analysis

To describe the breakthrough dynamics in the rectangular channel, a full 3-D mathematical model was developed considering 3-D convection and diffusion in the mobile phase and 2-D diffusion in the solid phase. For the systems considered, the axial diffusion component in the solid phase can be neglected, based on the order of magnitude estimate argument presented in the previous section. The mass balance in the mobile phase is

$$\frac{\partial c}{\partial t} - D_M \frac{\partial^2 c}{\partial z^2} - D_M \frac{\partial^2 c}{\partial x^2} - D_M \frac{\partial^2 c}{\partial y^2} + v(x, y) \frac{\partial c}{\partial z} = 0 \quad (15)$$

In Eq. 15, the velocity profile v(x,y), is obtained from

$$v(x, y) = \frac{4 \cdot \alpha \cdot K_V(x/d, y/d)}{\int_{-1}^{1} \int_{-\alpha}^{\alpha} K_V d\xi d\psi} \cdot v_{\text{ave}} \quad (16)$$

where[18]

$$K_V(\xi, \psi) = \frac{1}{2}(1 - \psi^2) - \sum_{n=0}^{\infty} \frac{16(-1)^n}{(2n+1)^3 \pi^3} \frac{\cosh\left(\frac{2n+1}{2}\pi\xi\right)}{\cosh\left(\frac{2n+1}{2}\pi\alpha\right)} \cos\left(\frac{2n+1}{2}\pi\psi\right) \quad (17)$$

The mass balance in the solid phase is given by

$$\frac{\partial q}{\partial t} = D_S \left(\frac{\partial^2 q}{\partial x^2} + \frac{\partial^2 q}{\partial y^2} \right) \quad (18)$$

To close the problem, we need to introduce a set of boundary conditions. In order to minimize the computational effort it is useful to consider that the problem has two planes of symmetry and it is, therefore, necessary to simulate the solution only for one fourth of the geometry. For the implementation of the solution in the commercial code gPROMS[19], it is also necessary to subdivide the numerical grid into four individual domains: the fluid phase, the solid corner, and the two sides of the solid. These four domains are shown in Figure 1.

Therefore, the set of boundary conditions is given by the equilibrium at the surface

$$q|_{y=d} = K \cdot c|_{y=d} \quad \text{for} \quad 0 < x < b \quad (19)$$

$$q|_{x=b} = K \cdot c|_{x=b} \quad \text{for} \quad 0 < y < d \quad (20)$$

continuity of the mass flux at the fluid-solid interface

$$D_M \left.\frac{\partial c}{\partial y}\right|_{y=d-} = D_S \left.\frac{\partial q}{\partial y}\right|_{y=d+} \quad \text{for} \quad 0 < x < b \quad (21)$$

$$D_M \left.\frac{\partial c}{\partial x}\right|_{x=b-} = D_S \left.\frac{\partial q}{\partial y}\right|_{x=b+} \quad \text{for} \quad 0 < y < d \quad (22)$$

continuity of concentration and mass flux at the solid-solid interfaces

$$q|_{y=d-} = q|_{y=d+}, \left.\frac{\partial q}{\partial y}\right|_{y=d-} = \left.\frac{\partial q}{\partial y}\right|_{y=d+} \quad \text{for} \quad b < x < b + w \quad (23)$$

$$q|_{x=b-} = q|_{x=b+}, \left.\frac{\partial q}{\partial x}\right|_{x=b-} = \left.\frac{\partial q}{\partial x}\right|_{x=b+} \quad \text{for} \quad d < y < d + w \quad (24)$$

The average concentration in the mobile phase can be calculated as follows

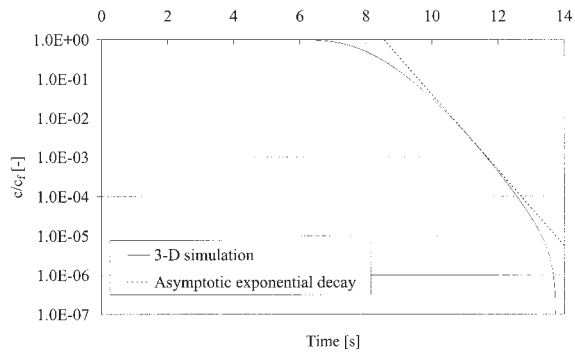

Figure 4. Determination of the asymptotic exponential decay approximating the breakthrough curve obtained from 3-D simulation for the calculation of the second moment (simulation for liquid flow at a velocity of 1.5 mm/s in the square channel).

Table 2. Summary of the Parameters Used for the HETP Calculation and the Numerical Simulation in the Gas Flow Through the Rectangular Channel[21]

Length of the column, L (m)	0.5
Half height of the mobile dimension, d (μm)	684
Half width of the mobile dimension, b (μm)	
Aspect ratio = 1	684
Aspect ratio = 10	6840
Half thickness of the solid phase, w (μm)	140
Corrected half thickness of the solid phase, w_C (μm)	
Aspect ratio = 1	154
Aspect ratio = 10	143
Void fraction, ε (−)	
Aspect ratio = 1	0.689
Aspect ratio = 10	0.813
Equilibrium constant of linear isotherm, K (−)	40
Retention factor, k (−)	
Aspect ratio = 1	18.05
Aspect ratio = 10	9.173
Diffusivity in the mobile phase, D_M (m^2/s)	$1.7\ 10^{-5}$
Diffusivity in the solid phase, D_S (m^2/s)	$7.4\ 10^{-10}$

$$c_{ave}(z,t) = \frac{1}{b \cdot d \cdot v_{ave}} \int_0^d \int_0^b c \cdot v(x,y)dxdy \tag{25}$$

From a series of breakthrough simulations, the first and second moments are calculated directly by integration, and for a desorption experiment

$$1^{st}\text{ Moment: } \mu = \int_0^\infty c_{ave}/c_f dt \tag{26}$$

$$2^{nd}\text{ Moment: } \sigma^2 = 2\int_0^\infty c_{ave}/c_f t \cdot dt - \mu^2 \tag{27}$$

The HETP can be obtained from

$$H = \frac{\sigma^2}{\mu^2} \cdot L \tag{28}$$

The 1st moment can be used to check the closure of the mass balance for the numerical solution since it represents the mean residence time.

$$\mu = \frac{L}{v_{ave}\varepsilon}[\varepsilon + (1-\varepsilon)K] \tag{29}$$

All simulations were performed using gPROMS 2.1.1 on a Pentium 4 - 1.7 GHz PC. The final time was selected as twice the 1st moment.

While the 1st moment is not affected by random numerical oscillations, the 2nd moment is strongly affected and increases with the integration time. This spurious effect can be avoided by observing the dimensionless output concentration in a semilogarithmic plot vs. time. The solution should tend to an asymptotic exponential decay,[20] and from the inspection of the curve, the tail can be integrated analytically. From the numerical simulations, the dimensionless concentration interval 0.01–0.001 was used in all calculations as it clearly showed the exponential decay. Figure 4 shows an example of the asymptotic exponential decay obtained from the numerical solution. The numerical error affects the solution for values of the dimensionless concentration below 10^{-3}, but the solution above this threshold allows the definition of the analytical exponential decay approximation.The second moment is calculated from

$$\sigma^2 = 2\int_0^{t_0} c_{ave}/c_f t \cdot dt + \frac{2a}{b}\exp(-bt_0)\left(t_0 + \frac{1}{b}\right) - \mu^2 \tag{30}$$

Representative gaseous system: carbon dioxide in a carbon monolith

To test the validity of the proposed HETP equation, the full numerical solution is used to predict the breakthrough curve in a channel of a carbon monolith. This system has been studied experimentally by Brandani et al.[21], and the physical constants and the dimensions of the channel are summarized in Table 2. Although the monolith consists of square channels, the numer-

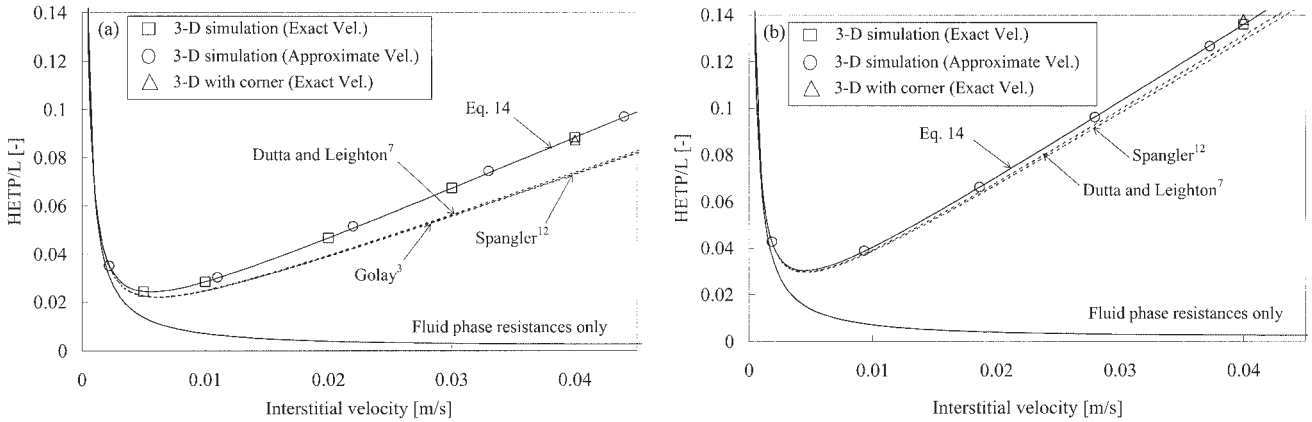

Figure 5. Variation with flow rate of the HETP values calculated from various theoretical models and the numerical breakthrough simulations for a gas system.

(a) square channel, and (b) rectangular channel with aspect ratio 10.

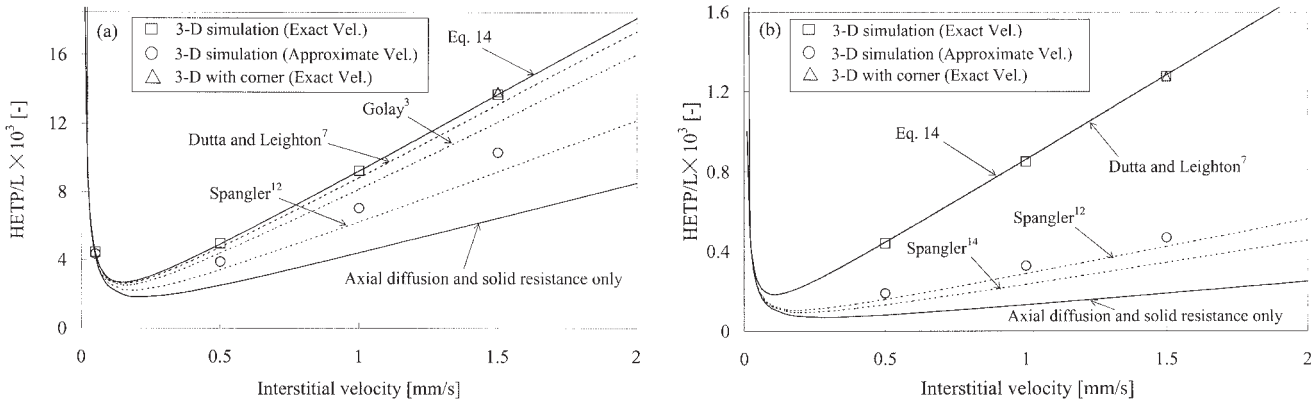

Figure 6. Variation with flow rate of the HETP values calculated from various theoretical models and the numerical breakthrough simulations for a liquid system.

(a) square channel, and (b) rectangular channel with aspect ratio 10.

ical simulations have been extended also to verify the effect of the aspect ratio, α.

Figure 5 shows the comparison between the full 3-D numerical solution and Eq. 14. At the highest flow rate, the numerical simulations include both solid geometries depicted in Figure 3. This comparison indicates that the simple redistribution of the solid from the corners to the side walls captures the additional mass transfer resistance accurately. The simulations were also carried out, for the geometry without corners, with the approximate velocity profile of Spangler[12]

$$K_V(\xi, \psi) = -\frac{1}{2}\cdot\frac{(\xi^2-\alpha^2)(\psi^2-1)}{(\xi^2-\alpha^2)+(\psi^2-1)} \tag{31}$$

For this particular application, the model predictions show that most of the dispersion can be attributed to the diffusion into the solid, that is, the second term in the HETP equation. Therefore, to enhance this process, it would be necessary to reduce the wall thickness of the monolith channels. The velocity profile plays a minor role in gas phase systems and the predictions from the solution obtained by Golay[3], Spangler[12], and Dutta and Leighton[7] are in close agreement. The deviation between these predictions and the full solution can be attributed to the effect of the solid material in the four corners. As can be seen from Figure 5b, the same considerations apply to an aspect ratio of 10, and all the models will tend to correctly predict the HETP as the aspect ratio is increased further.

Table 3. Summary of the Parameters Used for the HETP Calculation and the Numerical Simulation in the Liquid Flow Through the Rectangular Channel

Length of the column, L (m)	
Aspect ratio = 1	0.01
Aspect ratio = 10	0.20
Half height of the channel, d (μm)	20
Half width of the channel, b (μm)	
Aspect ratio = 1	20
Aspect ratio = 10	200
Half thickness of the solid phase, w (μm)	2
Corrected half thickness of the solid phase, w_c (μm)	
Aspect ratio = 1	2.10
Aspect ratio = 10	2.02
Void fraction, ε (−)	
Aspect ratio = 1	0.826
Aspect ratio = 10	0.900
Equilibrium constant of linear isotherm, K (−)	1.0
Retention factor, k (−)	
Aspect ratio = 1	0.210
Aspect ratio = 10	0.111
Diffusivity in the mobile phase, D_M (m^2/s)[22]	$1.0\ 10^{-9}$
Diffusivity in the solid phase, D_S (m^2/s)	$1.0\ 10^{-11}$

Representative liquid system: a dilute liquid in a microchannel

Figure 6 shows the HETP values for a liquid flow in square and rectangular channels with aspect ratios of 1 and 10, respectively. The details of this system are presented in Table 3. In the liquid system, the fluid phase diffusivity is several orders of magnitude smaller that the corresponding gas phase resistance and the equilibrium constant is of the order of unity. In this case, for the square channel, the dispersion of the concentration wave front is strongly affected by both the resistance in the fluid phase and the diffusion in the solid phase, that is, the last two terms in the HETP equation.

The difference in the HETP calculated from Eq. 14 and Dutta and Leighton[7] is again attributable to the effect of adsorption in the four corners and the need to define a corrected

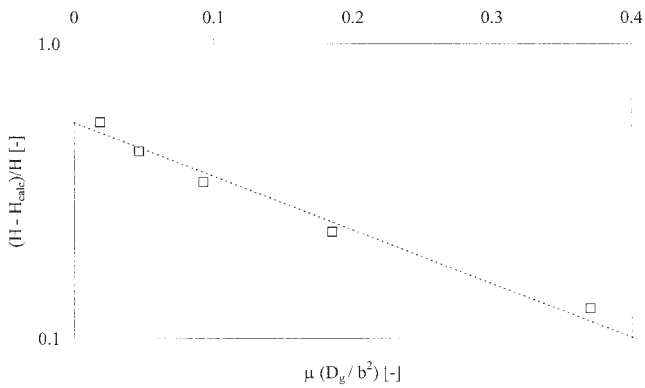

Figure 7. Effect of the column length on the HETP of liquid flowing through the rectangular channel of aspect ratio 10.

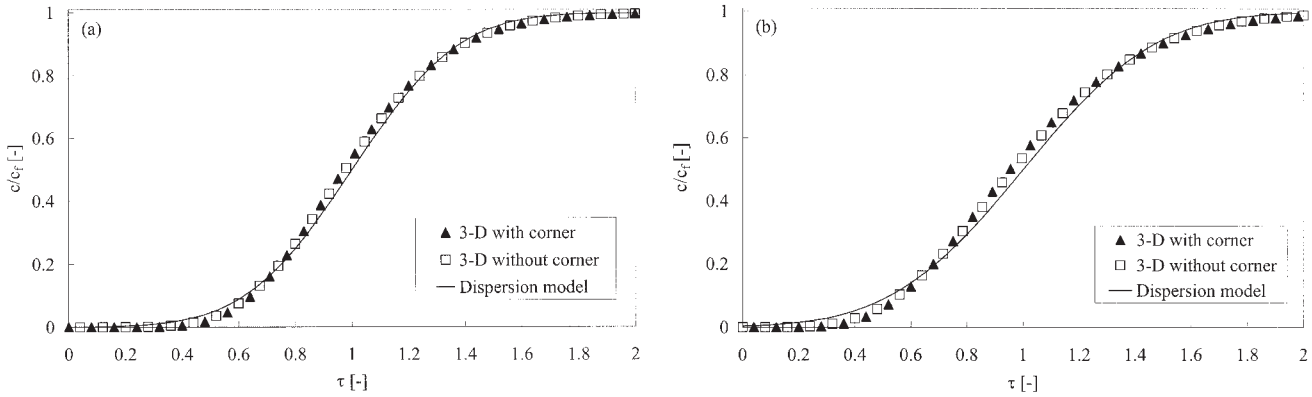

Figure 8. Breakthrough curves obtained from the 3-D mathematical model and calculated from the dispersion model, Eq. (32) at 0.04 m/s interstitial velocity for a gas system.

(a) square channel and (b) rectangular channel with aspect ratio 10.

wall thickness. Figure 6a shows that in this case the Golay[3] approximation underestimates the HETP, and it is evident that the approximate velocity profile proposed by Spangler[12] yields incorrect results for square channels.

For an aspect ratio of 10, Figure 6b, the effect of adsorption in the four corners becomes negligible and Eq. 14 reduces to the formulation of Dutta and Leighton[7]. Also in this case the approximate velocity profile of Spangler[12] provides a poor approximation to the exact solution.

The HETP approach is theoretically valid in the limit of a long column,[6] and the numerical solution allows us to check if this limit is achieved. The approach to the final dispersion will depend on the ratio of the mean residence time, that is, the first moment μ, and the largest time constant between w_c^2/D_S and b^2/D_M. In the four cases considered above, only the liquid phase simulation with an aspect ratio of 10 fell into a range where the limiting dispersion was not achieved fully for typical column lengths. Figure 7 shows the approach to the limiting dispersion as a function of the dimensionless group $\mu b^2/D_M$. The figure shows that relatively short columns, less than 1 cm, reach only 70 – 80% of the limiting HETP value and that there is a simple exponential approach. The criterion suggested by Dutta and Leighton[7], that 90% of the limiting dispersion is obtained for $L > 0.2 v_{ave} b^2/D_M$ (corresponding to $\mu b^2/D_M > 0.22$), is in reasonable agreement with our results.

Dynamics of breakthrough curves in gas systems

For the purposes of designing units the simple dispersion model[16] is often used to predict the breakthrough curve and for long columns it reduces to

$$\frac{c(\tau)}{c_f} = \frac{1}{2}\,\mathrm{erf}\left(\frac{1-\tau}{\sqrt{2H/L}}\right) \tag{32}$$

where $\tau = t/\mu$.

Figure 8 presents the comparison of the breakthrough curves obtained from the full numerical simulations and the desorption curve calculated from Eq. 32 for the gas system considered in this study. Although Eq. 32 represents a simple approximation, it clearly provides sufficient information for the purpose of designing a unit. If high purities are required, then the full numerical solution is needed to correctly predict the breakthrough times.

Figure 9 shows the same comparison for the liquid system.

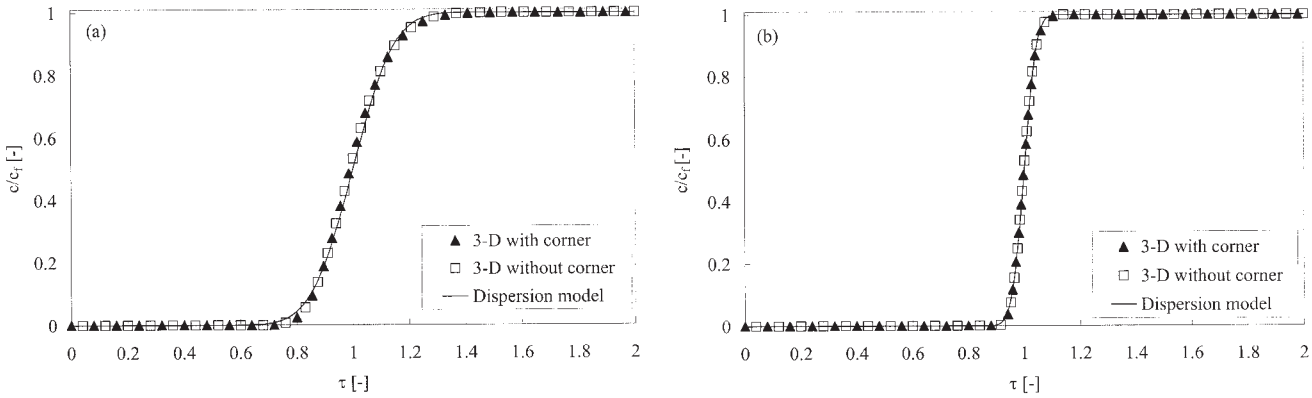

Figure 9. Breakthrough curves obtained from the 3-D mathematical model and calculated from the dispersion model, Eq. 32 at 1.5 mm/s interstitial velocity for a liquid system.

(a) 0.01 m long square channel, and (b) 0.20 m long rectangular channel with the aspect ratio 10.

Again the simple approximation calculated from Eq. 32 with the appropriate definition of the HETP terms yields a remarkably good result.

Conclusions

The breakthrough dynamics in a rectangular channel of arbitrary aspect ratio has been studied in detail. A new simple analytical equation is proposed for the prediction of the HETP of a chromatographic column, which has been validated against a full 3-D numerical model.

The aspect ratio has an effect on the dispersion in the fluid phase, as well as the solid phase. Simple interpolating functions are introduced to take into account the fluid phase dispersion in a rectangular channel of arbitrary aspect ratio. These functions converge to the limiting value only for $\alpha > 50$.

The effect of the aspect ratio on the dispersion due to the solid phase can be captured by a simple predictive approach, considering the four corners of the channels. By redistributing the solid from the corners to the sides, that is, increasing the mass transfer resistance, the additional dispersion can be predicted correctly.

The general HETP equation can be applied to a wide variety of sorbate-sorbent systems. In the case of a gas system, the main contribution to dispersion is typically caused by the resistance in the solid phase, and the effect of the velocity profile plays a minor role. For liquid systems, the largest contribution to the HETP comes from the resistance in the mobile phase due to the reduction in the fluid phase diffusion coefficient, and the lower value of the equilibrium constant.

For both gaseous and liquid systems the proposed HETP equation was shown to provide very accurate approximations to the values found from the full 3-D numerical simulations. This work has answered the need for simple equations to be applied in the analysis and design of chromatographic columns characterized by rectangular channels of adsorbent material. It is possible to identify the main contributions of the dispersion in the breakthrough curves and modify where needed the channel dimensions or the wall thicknesses. In the design of microchannel columns for liquid application, to improve the separation efficiency, one can also consider modified laterally-etched geometries, such as those originally proposed by Golay[14] and investigated in detail by Dutta and Leighton[7].

Acknowledgments

Financial support from the Leverhulme Trust (Philip Leverhulme Prize), and the Post-doctoral Fellowship Program of then Korea Science & Engineering Foundation (KOSEF), is gratefully acknowledged.

Notation

A,B,C = parameters in Eq. 6
b = half width of the rectangular channel, mm
c = concentration in the mobile phase, mol/m^3
$\bar{C}_M$ = Dimensionless resistance to mass transfer in the mobile phase
d = half height of the rectangular channel, mm
D_M = diffusivity in the mobile phase, m^2/s
D_S = diffusivity in the solid phase, m^2/s
F = volumetric flow rate, m^3/s
H = height equivalent to a theoretical plate, HETP, m
k = partition coefficient
K = equilibrium constant of linear isotherm
K_V = channel permeability, m^2
K_Q = channel permeability for volumetric flow, m^4
L = column length, m
q = concentration in the solid phase, mol/m^3
v = velocity, m/s
w = half thickness of the solid phase, m
w_C = corrected half thickness of the solid phase, m
x = distance along the horizontal direction, m
y = distance along the vertical direction, m
z = distance along the axial direction, m
t = time

Greek letters

α = aspect ratio (b/d)
ε = void fraction of rectangular channel
μ = first moment, s
σ^2 = second moment, s^2
ξ = dimensionless distance along the horizontal direction, x/d
ψ = dimensionless distance along the vertical direction, y/d
ζ = dimensionless distance along the axial direction, z/L

Superscript and subscript

ave = average value in the channel
calc = calculated value from numerical simulation
f = feed

Literature Cited

1. Ruthven DM, Thaeron C. Performance of a parallel passage adsorbent contactor. *Gas Separation and Purification*. 1996;10:63-73.
2. Ruthven DM. Past progress and future challenges in adsorption research. *Ind Eng Chem Res*. 2000;39:2127-2131.
3. Golay MJE. *Theory of Chromatography in Open and Coated Tubular Columns with Round and Rectangular Cross-Sections. Gas Chromatography.* New York:Academic Press; 1958;36-55.
4. Eiceman GA, Gardea-Torresdey J, Overton E, Carney K, Dorman F. *Gas Chromatography Anal Chem*. 2002;74:2771-2780.
5. Taylor G. Dispersion of soluble matter in solvent flowing slowly through a tube. *Proc R Soc London*. 1953;A219:186-203.
6. Aris R. On the dispersion of a solute in a fluid flowing through a tube. *Proc R Soc London*. 1956;A235:67-77.
7. Dutta D, Leighton DT. Dispersion in large aspect ratio microchannels for open-channel liquid chromatography. *Anal Chem*. 2003;75:57-70.
8. Zhang X, Regnier FE. Analysis of channel-geometry effects on separation efficiency in rectangular-capillary electrochromatography columns. *J Chromatography A*. 2000;869:319-328.
9. Desmet G, Baron GV. Chromatographic explanation for the side-wall Induced band broadening in pressure-driven and shear-driven flows through channels with a high aspect-ratio rectangular cross-section. *J Chromatography A*. 2002;946:51-58.
10. Terry SC, Jerman JH, Angell JB. A Gas chromatographic air analyzer fabricated on a silicon wafer. *IEEE Trans Electron Dev*. 1979;26:1880-1886.
11. Reston RR, Kolesar ESJ. Silicon-micromachined gas chromatography system used to separate and detect ammonia and nitrogen dioxide - Part I: Design, fabrication, and integration of the gas chromatography system. *J MEMS*. 1994;3:134-146.
12. Spangler GE. Height equivalent to a theoretical plate theory for rectangular GC columns. *Anal Chem*. 1998;70:4805-4816.
13. Aris R. On the dispersion of a solute by diffusion, convection and exchange between phases. *Proc R Soc London*. 1959;A252:538-550.
14. Golay MJE. The height equivalent to a theoretical plate of retentionless rectangular tubes. *J Chromatography A*. 1981;216:1-8.
15. Spangler GE. Relationships for modelling the performance of rectangular gas chromatographic columns. *J Microcolumn Separations*. 2001;13:285-292.
16. Giddings JC, Chang JP, Myers MN, Davis JM, Caldwell KD. Capillary liquid chromatography in field flow fractionation-type channels. *J Chromatography A*. 1983;255:359-379.
17. Levenspiel O. *Engineering Flow and Heat Exchange*. London: Plenum Press, 1998:Chap 15.
18. Cornish RJ. Flow in a pipe of rectangular cross-section. *Proc R Soc London*. 1928;A120:691-700.

19. Process Systems Enterprise, Ltd. gPROMS Introductory User Guide. 1999.
20. Brandani S, Ruthven DM. Moment analysis of the zero length column method. *Ind Eng Chem Res*. 1996;35:315-319.
21. Brandani F, Rouse A, Brandani S, Ruthven DM. Adsorption kinetics and dynamic behaviour of a carbon monolith. *Adsorption*. 2004;10: 99-109.
22. Gzil P, Baron GV, Desmet G. Computational fluid dynamics simulations yielding guidelines for the ideal internal structure of monolithic liquid chromatography columns. *J Chromatography A*. 2003;991:169-188.
23. Chatwin PC, Sullivan PJ. The effect of aspect ratio on longitudinal diffusivity in rectangular channels. *J Fluid Mech*. 1982;120:347-358.

Appendix A

The velocity profile in a rectangular channel can be derived from

$$\frac{\partial^2 K_V(\xi,\,\psi)}{\partial \xi^2} + \frac{\partial^2 K_V(\xi,\,\psi)}{\partial \psi^2} = -1 \tag{A1}$$

with the no-slip boundary condition

$$K_V(\pm\alpha,\,\psi) = K_V(\xi,\,\pm 1) = 0 \tag{A2}$$

The solution can be obtained in terms of an infinite series[18]

$$K_V(\xi,\,\psi) = \frac{1}{2}\,(1-\psi^2) - \sum_{n=0}^{\infty} \frac{16(-1)^n}{(2n+1)^3\pi^3} \frac{\cosh\left(\frac{2n+1}{2}\,\pi\xi\right)}{\cosh\left(\frac{2n+1}{2}\,\pi\alpha\right)} \cos\left(\frac{2n+1}{2}\,\pi\xi\right) \tag{A3}$$

and

$$K_Q = \int\int K_V(\xi,\,\psi)d\xi d\psi = \frac{4}{3}\,\alpha - \sum_{n=0}^{\infty} \frac{256}{(2n+1)^5\pi^5} \tanh\left(\frac{2n+1}{2}\,\pi\alpha\right) \tag{A4}$$

Applying the method of moments to the general mass balance equations[6] it is possible to arrive at the following differential equation[7]

$$\frac{\partial^2 \Delta c(\xi,\,\psi)}{\partial \xi^2} + \frac{\partial^2 \Delta c(\xi,\,\psi)}{\partial \psi^2} = \mathrm{Pe}\left[\frac{1}{2\alpha(1+k)^2} - \frac{2K_V(\xi,\psi)}{(1+k)K_Q}\right] \tag{A5}$$

which has to be solved to determine the effective diffusion coefficient.

The problem can be split into the solution of two functions[7]

$$\frac{\partial^2 \Delta c_1(\xi,\,\psi)}{\partial \xi^2} + \frac{\partial^2 \Delta c_1(\xi,\,\psi)}{\partial \psi^2} = -\frac{\alpha+1}{\alpha} \tag{A6}$$

$$\frac{\partial^2 \Delta c_2(\xi,\,\psi)}{\partial \xi^2} + \frac{\partial^2 \Delta c_2(\xi,\,\psi)}{\partial \psi^2} = 1 - \frac{4\alpha K_V(\xi,\,\psi)}{K_Q} \tag{A7}$$

where

$$\Delta c = \mathrm{Pe}\left(\frac{k}{2(1+\alpha)(1+k)^2}\,\Delta c_1 + \frac{1}{2\alpha(1+k)}\,\Delta c_2\right) \tag{A8}$$

Equations A6 and A7 can be solved up to an arbitrary constant, which can be determined imposing that the functions Δc_1 and Δc_2 represent deviations from the mean value

$$\int_0^{\alpha}\int_0^{1} \Delta c_1(\xi,\,\psi)d\psi d\xi + \frac{k\alpha}{1+\alpha} \times \left(\int_0^{\alpha} \Delta c_1(\xi,\,1)d\xi + \int_0^{1} \Delta c_1(\alpha,\,\psi)d\psi\right) = 0 \tag{A9}$$

$$\int_0^{\alpha}\int_0^{1} \Delta c_2(\xi,\,\psi)d\psi d\xi + \frac{k\alpha}{1+\alpha} \times \left(\int_0^{\alpha} \Delta c_2(\xi,\,1)d\xi + \int_0^{1} \Delta c_2(\alpha,\,\psi)d\psi\right) = 0 \tag{A10}$$

Δc_1 is readily obtained[7]

$$\Delta c_1(\xi,\,\psi) = -\frac{\xi^2+\alpha\psi^2}{2\alpha} + \frac{1}{6}\,\frac{\alpha(\alpha+1)^2 + k\alpha(\alpha^2+6\alpha+1)}{\alpha(\alpha+1)(1+k)} \tag{A11}$$

and g_1 is obtained from

$$g_1 = \frac{12}{\alpha+1}\int_0^{\alpha}\int_0^{1} \Delta c_1(\xi,\,\psi)d\psi d\xi - \frac{12\alpha}{(\alpha+1)^2} \times \left(\int_0^{\alpha} \Delta c_1(\psi,\,1)d\xi + \int_0^{1} \Delta c_1(\alpha,\,\psi)d\psi\right) \tag{A12}$$

which gives

$$g_1 = \frac{2\alpha^2}{(\alpha+1)^2} \tag{A13}$$

To solve for Δc_2 , we follow the procedure of Chatwin and Sullivan[23] and express in terms of a Fourier series of cosines

$$1 - \frac{4\alpha}{K_Q}\,K_V(\xi,\,\psi) = \sum_{m=0}^{\infty}\sum_{p=0}^{\infty} a_{m,p}\cos(m\pi\psi)\cos\left(p\pi\,\frac{\xi}{\alpha}\right) \tag{A14}$$

where

$$a_{0,0} = 0$$

$$a_{m,0} = -\frac{8\alpha(-1)^m}{m^2\pi^2 K_Q} \times \left[1 + \frac{2m^2}{\alpha\pi^3}\sum_{n=0}^{\infty}\frac{\tanh\left(\frac{2n+1}{2}\pi\alpha\right)}{\left(\frac{2n+1}{2}\right)^3}\frac{1}{\left(\frac{2n+1}{2}\right)^2 - m^2}\right]$$

$$a_{0,p} = -\frac{16\alpha^2(-1)^p}{\pi^5 K_Q}\sum_{n=0}^{\infty}\frac{\tanh\left(\frac{2n+1}{2}\pi\alpha\right)}{\left(\frac{2n+1}{2}\right)^3}\frac{1}{\alpha^2\left(\frac{2n+1}{2}\right)^2 + p^2}$$

$$a_{m,p} = -\frac{32\alpha^2(-1)^{m+p}}{\pi^5 K_Q} \sum_{n=0}^{\infty}\frac{\tanh\left(\frac{2n+1}{2}\pi\alpha\right)}{\left(\frac{2n+1}{2}\right)}\frac{1}{\left(\frac{2n+1}{2}\right)^2 - m^2}\frac{1}{\alpha^2\left(\frac{2n+1}{2}\right)^2 + p^2}$$

If we express Δc_2 in terms of a Fourier series of cosines

$$\Delta c_2(\xi, \psi) = \sum_{m=0}^{\infty}\sum_{p=0}^{\infty} A_{m,p}\cos(m\pi\psi)\cos\left(p\pi\frac{\xi}{\alpha}\right) \quad \text{(A15)}$$

the boundary conditions are automatically fulfilled and for m and p nonzero

$$A_{m,0} = -\frac{a_{m,0}}{m^2\pi^2}$$

$$A_{0,p} = -\frac{a_{0,p}\alpha^2}{p^2\pi^2}$$

$$A_{m,p} = -\frac{a_{m,p}}{m^2\pi^2 + p^2\pi^2/\alpha^2}$$

Substituting in Eq A10 we can solve for the unknown constant term

$$A_{0,0} = -\frac{k}{1+k}\frac{1}{\alpha+1}\left[\sum_{m=1}^{\infty}(-1)^m A_{m,0} + \sum_{p=1}^{\infty}(-1)^p A_{0,p}\right] \quad \text{(A16)}$$

The function g_2 can be obtained from

$$g_2 = \frac{210}{\alpha}\int_0^{\alpha}\int_0^1 K_V(\xi, \psi)\Delta c_2(\xi, \psi)d\psi d\xi - \frac{210}{\alpha}\left(\int_0^{\alpha}\Delta c_2(\xi, 1)d\xi + \int_0^1 \Delta c_2(\alpha, \psi)d\psi\right) \quad \text{(A17)}$$

which gives

$$g_2 = \frac{210}{K_Q}\left[\frac{\alpha}{\pi^4}\sum_{m=1}^{\infty}\frac{(-1)^m}{m^4}a_{m,0} + \frac{2}{\pi^7}B_m + \frac{2\alpha^4}{\pi^7}B_p + \frac{2\alpha^2}{\pi^7}B_{mp}\right] \quad \text{(A18)}$$

where

$$B_m = \sum_{m=1}^{\infty}\frac{(-1)^m}{m^2}a_{m,0}\sum_{n=0}^{\infty}\frac{\tanh\left(\frac{2n+1}{2}\pi\alpha\right)}{\left(\frac{2n+1}{2}\right)^3}\frac{1}{\left(\frac{2n+1}{2}\right)^2 - m^2}$$

$$B_p = \sum_{p=1}^{\infty}\frac{(-1)^p}{p^2}a_{0,p}\sum_{n=0}^{\infty}\frac{\tanh\left(\frac{2n+1}{2}\pi\alpha\right)}{\left(\frac{2n+1}{2}\right)^3}\frac{1}{\alpha^2\left(\frac{2n+1}{2}\right)^2 + p^2}$$

$$B_{mp} = \sum_{m=1}^{\infty}\sum_{p=1}^{\infty}\frac{(-1)^{m+p}}{m^2 + p^2/\alpha^2}a_{m,p} \times \sum_{n=0}^{\infty}\frac{\tanh\left(\frac{2n+1}{2}\pi\alpha\right)}{\left(\frac{2n+1}{2}\right)}\frac{1}{\alpha^2\left(\frac{2n+1}{2}\right)^2 + p^2}\frac{1}{\left(\frac{2n+1}{2}\right)^2 - m^2}$$

The function g_3 can be obtained from

$$g_3 = \frac{30}{\alpha+1}\int_0^{\alpha}\int_0^1 [K_V(\xi, \psi) - 1]\Delta c_1(\xi, \psi)d\psi d\xi + \frac{30}{\alpha}\int_0^{\alpha}\int_0^1 \Delta c_2(\xi, \psi)d\psi d\xi - \frac{30}{\alpha+1} \times \left(\int_0^{\alpha}\Delta c_2(\xi, 1)d\xi + \int_0^1 \Delta c_2(\alpha, \psi)d\psi\right) \quad \text{(A19)}$$

which gives

$$g_3 = \frac{30}{\alpha+1}\left[\frac{\alpha(\alpha+1)}{24} - \frac{\alpha^2}{K_Q}\left(\frac{1}{30} + \frac{\alpha}{18}\right) + C_n + \sum_{m=1}^{\infty}(-1)^m\frac{\alpha A_{m,0}}{4} + \sum_{p=1}^{\infty}(-1)^p\frac{A_{0,p}}{4}\right] \quad \text{(A20)}$$

where

$$C_n = \frac{2\alpha}{K_Q \pi^6} \sum_{n=0}^{\infty} \frac{\frac{1}{2}\left(\frac{2n+1}{2}\right)^2 \pi^2 \alpha(\alpha+1) + 1 - \alpha}{\left(\frac{2n+1}{2}\right)^7 \pi\alpha} \times \tanh\left(\frac{2n+1}{2}\pi\alpha\right) - \frac{(-1)^n}{\left(\frac{2n+1}{2}\right)^6}$$

Appendix B

In the 3-D numerical simulation, all the mass balance equations were converted into dimensionless form using the following dimensionless variables and parameters

$$C = \frac{c}{c_f}, \quad C_{\text{ave}} = \frac{c_{\text{ave}}}{c_F} \quad Q = \frac{q}{q_F} = \frac{q}{Kc_F},$$

$$\tau = \frac{t}{\mu}, \quad \xi = \frac{x}{d}, \quad \psi = \frac{y}{d}, \quad \zeta = \frac{z}{L}, \quad V = \frac{v}{v_{\text{ave}}},$$

$$\text{Pe}_M = \frac{D_M}{v_{\text{ave}} L}, \quad \text{Pe}_S = \frac{D_S}{v_{\text{ave}} L}, \quad R_d = \frac{L}{d},$$

$$R_W = \frac{L}{w} \quad \sigma = \frac{(\varepsilon + (1-\varepsilon)K)}{\varepsilon} \tag{B1}$$

The mass balance in the mobile phase, Eq. 15, reduces to

$$\frac{\partial C}{\partial \tau} - \text{Pe}_M \sigma \frac{\partial^2 C}{\partial \zeta^2} - \text{Pe}_M R_d^2 \sigma \frac{\partial^2 C}{\partial \xi^2} - \text{Pe}_M R_d^2 \sigma \frac{\partial^2 C}{\partial \psi^2} + V\sigma \frac{\partial C}{\partial \zeta} = 0 \tag{B2}$$

In the dimensionless domain, the velocity profile, Eq. 16, becomes

$$V(\xi, \psi) = \frac{4\alpha K_V}{\int_{-1}^{1}\int_{-\alpha}^{\alpha} K_V d\xi d\psi} \tag{B3}$$

The mass balance in the solid phase, Eq. 18, is changed into

$$\frac{\partial Q}{\partial \tau} = \text{Pe}_S R_d^2 \sigma \left(\frac{\partial^2 Q}{\partial \xi^2} + \frac{\partial^2 Q}{\partial \psi^2}\right) \tag{B4}$$

The boundary conditions, Eqs. 19 – 24, become

$$Q|_{\psi=1} = C|_{\psi=1} \quad \text{for} \quad 0 < \xi < \alpha \tag{B5a}$$

$$Q|_{\xi=\alpha} = C|_{\xi=\alpha} \quad \text{for} \quad 0 < \psi < 1 \tag{B5b}$$

$$\left.\frac{\partial C}{\partial \psi}\right|_{\psi=1-} = \frac{\text{Pe}_S}{\text{Pe}_M} \left.\frac{\partial Q}{\partial \psi}\right|_{\psi=1+} \quad \text{for} \quad 0 < \xi < \alpha \tag{B6a}$$

$$\left.\frac{\partial C}{\partial \xi}\right|_{\xi=\alpha-} = \frac{\text{Pe}_S}{\text{Pe}_M} \left.\frac{\partial Q}{\partial \xi}\right|_{\xi=\alpha+} \quad \text{for} \quad 0 < \psi < 1 \tag{B6b}$$

$$Q|_{\psi=1-} = Q|_{\psi=1+}, \quad \left.\frac{\partial Q}{\partial \psi}\right|_{\psi=1-} = \left.\frac{\partial Q}{\partial \psi}\right|_{\psi=1+} \quad \text{for} \quad \alpha < \xi < \alpha + \frac{R_d}{R_W} \tag{B7a}$$

$$Q|_{\xi=\alpha-} = Q|_{\xi=\alpha+}, \quad \left.\frac{\partial Q}{\partial \xi}\right|_{\xi=\alpha-} = \left.\frac{\partial Q}{\partial \xi}\right|_{\xi=\alpha+} \quad \text{for} \quad 1 < \psi < 1 + \frac{R_d}{R_W} \tag{B7b}$$

The dimensionless average concentration in the mobile phase is

$$C_{\text{ave}} = \frac{\int_0^{\alpha}\int_0^{1} C \cdot V d\psi d\xi}{\alpha} \tag{B8}$$

Manuscript received Mar. 30, 2004, and revision received Oct. 28, 2004.